http://journal.uir.ac.id/index.php/JGEET
E-ISSN : 2541-5794
P-ISSN : 2503-216X

Journal of Geoscience, Engineering, Environment, and Technology
Vol 04 No 02 2019

RESEARCH ARTICLE

Tidal Ellipses Analysis Based on Flow Model Hydrodynamic Data Acquisition in Mandeh Bay, West Sumatera

Ulung J. Wisha[1]*, Ruzana Dhiauddin[2], and Wisnu A. Gemilang[3]
[1]Research Institute for Coastal Resources and Vulnerability, Ministry of Marine Affairs and Fisheries, Indonesia

* Corresponding author : ulungjantama@kkp.go.id
Tel.: +62 751 751458; fax:+62 751 751458
Received: Mei 06, 2019; Accepted: Jun 19, 2019.
DOI: 10.25299/jgeet.2019.4.2.3115

Abstract

Mandeh Bay is threatened by sedimentation issue caused by the rapid development of marine tourism area which strongly impacts to the environmental degradation. Due to the semi-enclosed area of Mandeh Bay, the tidal current has a significant role in triggering vertical and horizontal transports within the bay. This study aimed to determine the characteristic of tidal current during the southwest monsoon. We developed a hydrodynamic model based on Navier-Stokes equations using a flexible mesh and tidal forecast in which the validation is performed by ADCP data. The simulation results will be used as the basic data to develop a model which depicts the elliptical pattern of tidal current constituents. Offshore rotary tidal currents which are originally semidiurnal reiterate the elliptical pattern every 6 hours and 12 minutes. The strongest semidiurnal current speeds are observed in the bay mouth ranged from 0.1-0.5 m.s-1. The tidal constituent ellipses are oriented more meridionally and in several areas oriented zonally. The current speed of M_2 is the highest at all which the S_2 speed is averagely one third of M_2 magnitude. While, the two main diurnal tidal constituents (K_1 and O_1) have the maximum speeds approximately one fifth of M_2 magnitude. Thus, the domination of semidiurnal constituents may trigger sediment distribution and accumulation within the bay because of its twice tidal oscillations entering the bay.

Keywords: Tidal current, Mandeh Bay, southwest monsoon, hydrodynamic model, tidal current ellipses

1. Introduction

West Sumatera is one of the provinces that has potential marine ecotourism enhancing local income (Hermon, 2016).The rapid development of West Sumatera has a role in inducing environmental degradation. Several coastal damages, caused by mass-tourism, discrepant land-use, and industrial activities, have been occurring. This may enhance the sedimentations, pollutions, marine litters issues, and coastal vulnerability as well (Duhec et al., 2015). According to its positions, West Sumatera waters are tremendously strategic which are directly bordered by the Indian Ocean. This condition contributes to the generation of local water mass movement related to sedimentary behavior (Hanebuth et al., 2015). One of the significant areas in the West Sumatera experiencing dramatic sedimentation issues is Mandeh Bay.

In Mandeh Bay, the existence of several new ports and settlements is the main problems of ineffective development. Due to the rapid development that has been occurring, sedimentation issue strongly threats the condition within the bay which induces the high level of turbidity and water quality degradation as well. Mandeh Bay is a semi-enclosed water area which depends on hydrodynamic regime such as tidal current (Hidayat and Rozamuri, 2016). Water mass movement is a complex phenomenon which is related to the controlling factors variation generating sea current, so that the regime of tidal current is essential to study because it is the main factor triggering transport mechanism (Chen et al., 2015), especially for Mandeh Bay where the water mass movement tends to be weak due to its semi-enclosed water area. This may cause sedimentation. Sediment sourced from estuaries and rivers will take place triggering the higher suspended sediment concentration in water (Bábek et al., 2015).

The study about current pattern correlated with the tidal regime is a significant way to depict the water circulation within a bay. In the narrowed and semi-enclosed water area, tidal is the primary factor inducing water mass circulation (Wang et al., 2018). Tidal current is a physical factor that always changes depending on the monsoon conditions (Rath et al., 2017). It is obvious why tidal current characteristics in Mandeh Bay is necessary to determine the transport mechanism and water dynamics for better development in the future. Moreover, this study may helpful for fisheries and shipping activities in term of sea current dynamics. One of the ways to Fig. out the tidal current pattern is model approach using numerical simulation. This approach can illustrate vastly the study area that may be uncovered by

observation. This study aimed to determine the tidal current condition during the southwest monsoon.

2. Materials and Methods

2.1 Field measurement and Flow model simulation

Field observation was conducted in June 2018. We used ADCP (Acoustic Doppler Current Profiler) to collect current, and tidal data which those data will be used for validating the simulation results. Unfortunately, Due to a technical problem, ADCP data cannot be retrieved. So, we decided to use the older ADCP data that were obtained from another survey project of the Research Institute for Coastal Resources and Vulnerability (RICRV) in June 2015. Bathymetry data obtained from the single-beam echosounder survey and Global Tide Prediction data were applied as the model input. Simulation results will illustrate as a tidal current pattern for four extreme tidal conditions which those results will be validated using field observation data. To evaluate the simulation results, we employed a Root Mean Squared Error (RMSE) formula as follows:

$$RMSE = \sqrt{\frac{1}{n}\sum_{i=1}^{n}(y - yi)^2} \quad (1)$$

Where:
n = total data validated
y = model result data
yi = observation data

Flow model flexible mesh was employed to simulate the tidal current pattern in the form of a two-dimensional hydrodynamic model. The model is based on the solution of incompressible Reynolds which is averaged by Navier-Stokes equations consist of continuity and momentum equations.

The local continuity equation is formulated as follows:

$$\frac{\partial u}{\partial x} + \frac{\partial v}{\partial y} + \frac{\partial w}{\partial z} = S \quad (2)$$

The two horizontal momentum equations for x and y components are generally written by the following discretization:

$$\frac{\partial u}{\partial t} + \frac{\partial u^2}{\partial x} + \frac{\partial vu}{\partial y} + \frac{\partial wu}{\partial z} = fv - g\frac{\partial \eta}{\partial x} - \frac{1}{\rho_o}\frac{\partial P_a}{\partial x} - \frac{g}{\rho_o}\int_z^\eta \frac{\partial \rho}{\partial x}dz - \frac{1}{\rho_o h}\left(\frac{\partial S_{xx}}{\partial x} + \frac{\partial S_{xy}}{\partial y}\right) + Fu + \frac{\partial}{\partial z}\left(vt\frac{\partial u}{\partial z}\right) + U_s \quad (3)$$

$$\frac{\partial v}{\partial t} + \frac{\partial v^2}{\partial y} + \frac{\partial uv}{\partial x} + \frac{\partial wv}{\partial z} = -fu - g\frac{\partial \eta}{\partial y} - \frac{1}{\rho_o}\frac{\partial P_a}{\partial y} - \frac{g}{\rho_o}\int_z^\eta \frac{\partial \rho}{\partial y}dz - \frac{1}{\rho_o h}\left(\frac{\partial S_{yx}}{\partial x} + \frac{\partial S_{yy}}{\partial y}\right) + Fv + \frac{\partial}{\partial z}\left(vt\frac{\partial v}{\partial z}\right) + V_s S \quad (4)$$

Where:

t	: time
x, y, z	: cartesian coordinate
η	: surface elevation
d	: still water depth
u, v, w	: velocity components in the x, y, and z direction
f	: $2\Omega sin\phi$ (Coriolis parameter)
g	: gravitational acceleration
ρ	: density
$S_{xx}, S_{xy}, S_{yx}, S_{yy}$	: components of radiation stress tensor
vt	: vertical turbulent or eddy viscosity
Pa	: atmospheric pressure
ρo	: reference density
S	: magnitude of discharge due to point sources
(U_s, V_s)	: velocity by which the water is discharged into the ambient water

Field measurement points of ADCP surveys are positioned within Mandeh Bay next to Cubadak Island (Fig. 1). ADCP was deployed for 30 days on June-July 2018 at 10 meters depth. We used ADCP Nortek that can record several physical parameters such as currents, tidal, and temperature data. After the acquisition stage has done, the data must be sorted using Surge Software to delete the bias data. Current data is recorded in several depth-cells data, we only used the uppermost data adjusted with the simulation built. Thus, between model and field data can be well compared to evaluate the error resulted from the simulation.

The simulation was running once for 15 days that represents 2 phases of tidal (neap and spring). We used tidal forecast data as the boundary conditions which are obtained from Naotide execution and three boundaries which represent north, west, and south tidal condition in the mesh file (Fig. 2). Model results will be shown spatially in the form of hydrodynamical maps for four extreme tidal conditions. The model set-up is shown in Table 1.

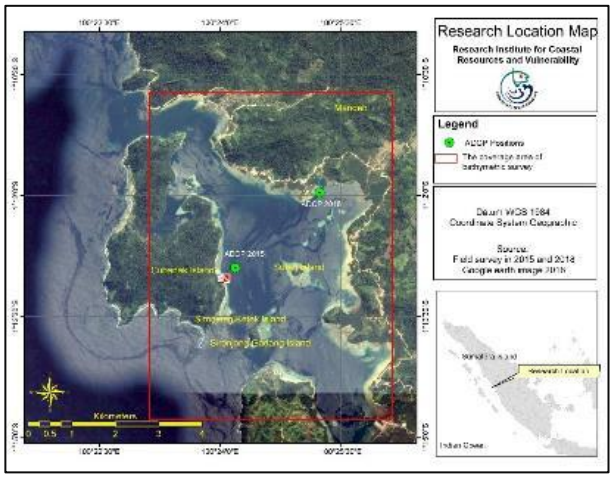

Fig. 1. Study area of Mandeh Bay.

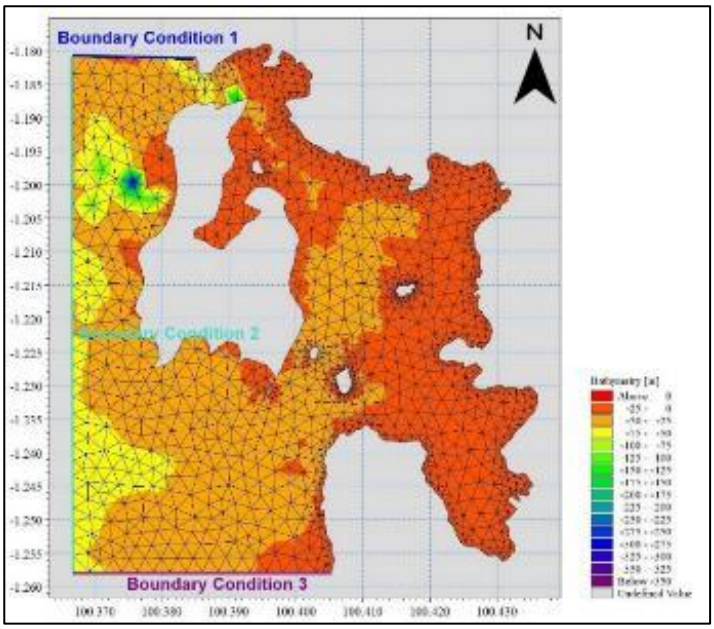

Fig. 2. Boundary condition and mesh file of hydrodynamic model.

Table 1. Model set-up for hydrodynamic simulation

Parameter	Implemented in the simulation
Time of simulation	Number of time step = 384 Time step interval = 3800 sec Simulation start date = 10/06/2018 12.00 AM Simulation end date = 26/06/2018 12.00 AM
Mesh boundary	Bathymetry = Hydrography and Oceanography Center, Indonesian Navy - Bathymetry map digitation
Flood and dry	Drying depth = 0.005 m Flooding depth = 0.05 m Wetting depth = 0.1 m
Wind forcing	Format = Varying in time, constant in domain Neutral pressure 103 hPa Soft start interval = 0 sec
Boundary condition	Type = Specified level Format = Varying in time, constant along boundary Time Series = Tide forecasting with coordinates below: 1. Longitude: 100.38600, Latitude: -1.2578 2. Longitude: 100.36669, Latitude: -1.2388 3. Longitude: 100.37596, Latitude: -1.1812

2.2 Tidal harmonic and ellipses analysis

Due to the limited ADCP measurement (only one instrument mounted), we developed a tidal current model to analyze the tidal current using tidal ellipse parameters which can sufficiently cover the study area. It is important to be able to extract the harmonic components of the current associated with the tide. Because of tidal current periodic nature, it can be separated into basic harmonic constituents. The longer the time series, the better the results will become, as the closely spaced can be more properly separated.

The harmonic analysis is based on a least-square fit of the observation area. This methodology essentially allows for the determination of the barotropic tide at any time at any location within the study area. The velocity components are represented by a mean current and sum of harmonic current constituents as follows:

$$\boldsymbol{u(r,t) = (r) + \sum_{i=1}^{N}[a_i(r)cos(\omega_i t) + b_i(r)sin(\omega_i t)]} \quad (5)$$

Where, u_o is the mean current, r(x,y) is the position vector, a_i and b_i are amplitudes, t is time, ω_i is the frequency of a given constituent, and N is the number of constituents. Before executing the least square fit, the data are multiplied with Gaussian weighting function on the form:

$$\phi(r, r_j) \sim exp\left\{-\left[\frac{(x-x_j)^2}{\sigma_x^2} + \frac{(y-y_j)^2}{\sigma_y^2}\right]\right\} \quad (6)$$

Where, r_j (x_j,y_j) are the positions of the knot points and σ_x and σ_y are decay parameters that control the shape of Gaussian curve. In this study, we used isotropic decay parameter with σ_x= σ_y= 55.5 km, which is equivalent to the length of half a degree latitude.

The tidal constituents that have been extracted, six principal constituents and three over-tides are shown

in Table 2. Results of extracted tidal currents are depicted in the form of tidal ellipse parameters which consist of semi-major and semi-minor axes representing maximum and minimum current speeds respectively, the inclination is the counterclockwise angle between the east direction and the semi-major axis. The ellipse parameters are illustrated using a concept of Greenwich phase lag by appointing each tidal constituent which the fictitious star will travel around the equator with an angular speed as its corresponding constituent (Fig. 3).

Table 2. Tidal constituents used in the harmonic analysis. Period is given in hours and frequency in cycles/day

Name of constituent	Symbol	Period	Frequency
Diurnal			
Luni-solar	K_1	23.83	1.00
Principal Lunar	O_1	26.78	0.93
Semi-Diurnal			
Smaller lunar elliptic	L_2	12.19	1.97
Principal lunar	M_2	12.41	1.93
Larger lunar elliptic	N_2	12.69	1.90
Principal solar	S_2	12.01	2.00
Higher harmonics			
Shallow water over-tides of principal lunar	M_4	6.21	3.86
	M_6	4.14	5.80
	M_8	3.11	7.73

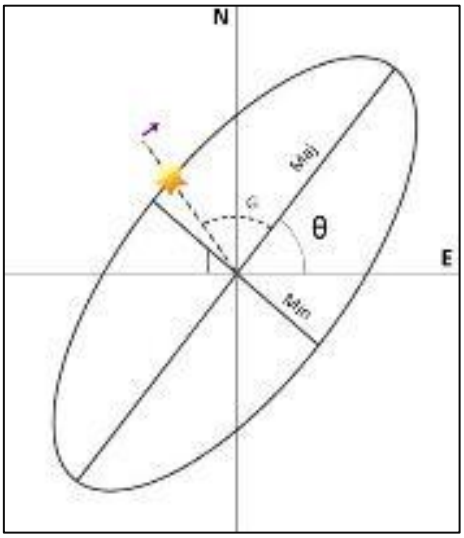

Fig. 3. Illustration of a clockwise rotating tidal current ellipse and its parameters. Modified from (Foreman, 1978) and (Vindenes et al., 2018).

3. Result and Discussion

3.1 Sea current profiles in Mandeh Bay

The dominance of current speed and direction is shown in the form of current rose (Fig. 4). ACDP was set for five cells measurement which each cell is representing the water column with specified depth (1.5 m, 3.5 m, 5.5 m, and 7.5 m from the surface). In the uppermost cell (1.5 m) near the surface, the dominance current flows southwestward (16%) and northeastward (12%) which the predominant current speed ranged from 0-0.1 m.s-1. Higher speed is also observed only ranged between 0.1-0.2 m.s-1 (2 %) and 0.2-0.3 m.s-1 (0.1%) respectively with the same direction domination. The deeper layer (3.5 m from the surface) shows the same current direction domination that is flowing southwestward (15.5 %) and northeastward (12.1 %). The current speed <0.1 m.s-1 is still dominant which the higher speed (ranging from 0.2-0.3 m.s-1) is observed flowing southwestward (0.1 %) while the current speed ranging from 0.1-0.2 m.s-1 is also identified in the same direction (0.5-1 %). At 5.5 m depth, the dominant current direction is oppositely changed in which the sea current flows predominantly northeastward (14 %) and southwestward (6 %). The current speed <0.1 m.s-1 is frequently identified in all directions and the higher speed (ranging from 0.2-0.3 m.s-1) is observed less than 1 %. The same condition is identified at 7.5 m depth which is the surface bottom. The current flows predominantly northeastward (17.5 %) and southwestward (12 %) which the current speed ranges between 0-0.2 m.s-1.

From the results above, it is interpreted that the current speed in the surface layer is the strongest which gradually becomes weaker in accordance with the increasing depth. This mechanism is common because, in the surface, the energy transfer from winds takes place generating higher speed in the surface while in the deeper layer, the wind force is gradually reduced by the detention of bottom friction and density so that the speed becomes weaker in the surface bottom.

The opposite condition between the surface and bottom layers shows the influence of spiral Ekman regime in which the current direction rotates counterclockwise in the southern hemisphere. The effect of the spiral Ekman results from Coriolis and wind forces which gradually forms spiral toward the bottom of waters and decreases speed. This event is the main factor triggering vertical transport in the ocean floor. Mandeh Bay becomes the area impacted this regime which the transport mechanism is following spiral Ekman mechanism, furthermore, the other physical factors also take place such as tidal, density, waves, bottom friction etc.

Vertical profiles of sea current are shown in Fig. 4 which are obtained from east velocity (x-direction), north velocity (y-direction) and up velocity (z-direction) of current. The negative velocity is representing the westward direction while the positive value is showing the eastward direction. From Fig. 5, sea current flows dominantly westward with the speed ranged 0-0.12 m.s-1. North velocity profile is showing the dominant direction which is southward with the current speed ranged 0-0.13 m.s-1. Up velocity profile tends to be stable along the decreasing depth with the weakest velocity ranged from 0-0.08 m.s-1. Furthermore, between 4.5-8.5 meters depth, the water mass moves averagely toward the bottom. Vertical profile of current is also reflecting the vertical transport mechanism in the Mandeh Bay.

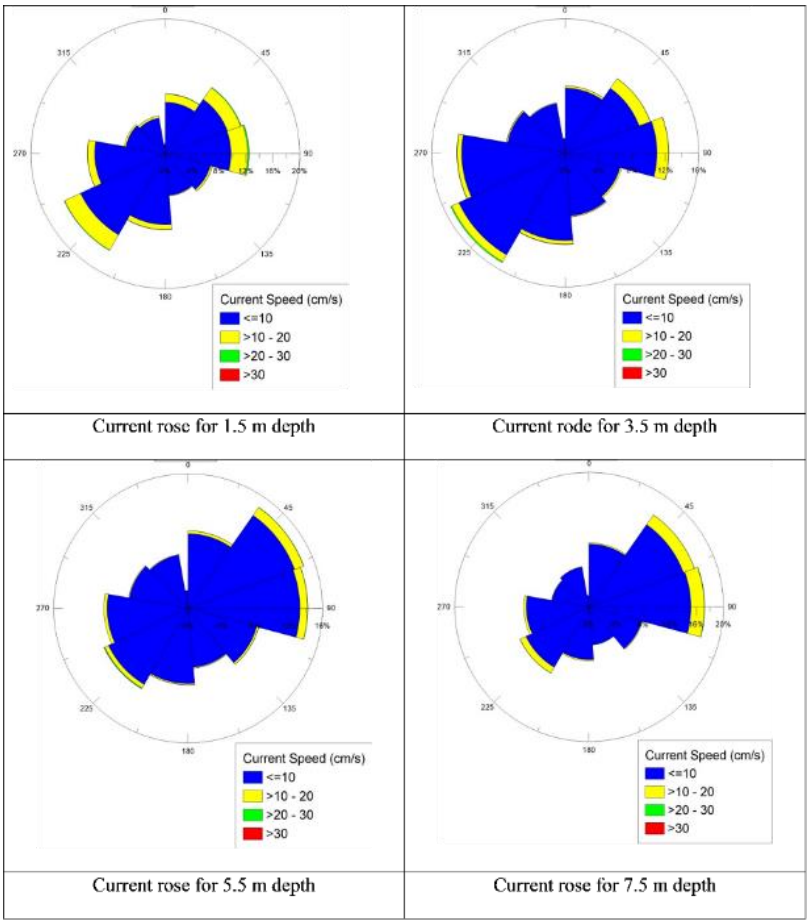

Fig. 4. Current rose for four depth layers based on ADCP measurement.

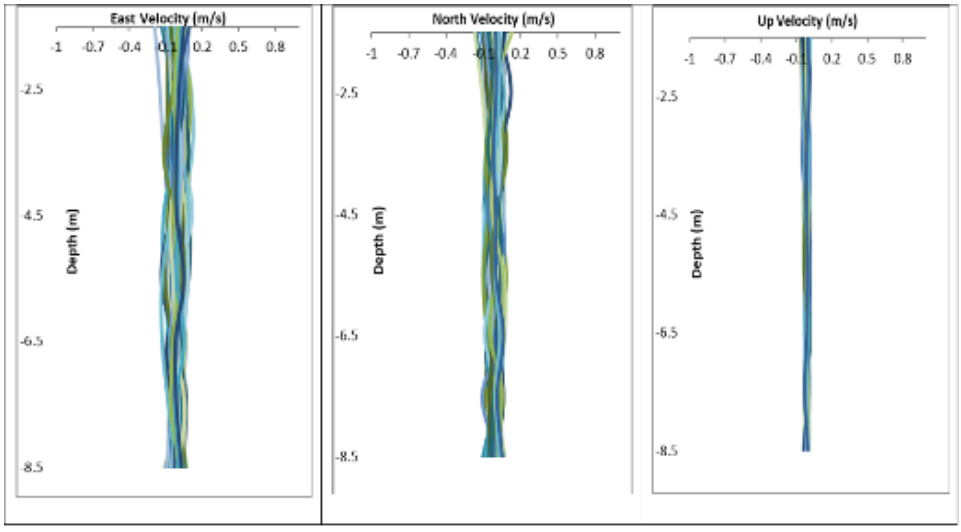

Fig. 5. Sea current's vertical profile in Mandeh Bay

3.2 Model Validation

The model validation is performed by comparing ADCP data and model result. In this study, we validated the surface elevation and velocity components (U and V) in the form of elliptical analysis. The comparison between field measurement data (red line) and the model result (blue line) shows the same surface elevation phases (Fig. 6). The RMSE calculated is 17.76 % which shows a slight error identified from the model developed. Based on the tidal measurement, the tidal type of Mandeh Bay is mixed tide prevailing semidiurnal, it was also determined by (Mukhtar et al., 2016).

There are some different phases according to model validation in Fig. 5 where the elevation is not uniform at the neap tidal condition (green ellipses). During the neap conditions, the astronomical forces become weaker than the spring conditions, resulting in the external forces predomination. That is why

during the neap tidal conditions, the fluctuation is more erratic (Qarnain et al., 2014).

Fig. 7 depicts the current velocity components comparison between the model result and field measurement in the form of vector magnitude and direction. The current velocity ranged from -0.2 up to 0.28 m.s-1 and from -0.1 up to 0.12 m.s-1 for field measurement and model result respectively. The direction differentiation approximately 15 degrees predominates east-northeastward and west-southwestward.

The ellipsoid velocity components analysis is also depicting that the tidal current is a rotary cycle which it rotates continuously 360 degrees during the tidal period. The rotation of tidal current is caused by the earth's rotation that changes the astronomical forces depended on its location, inducing the different current speed as the tidal regime takes place (Poulain, 2013). Moreover, the local factors also have a role in triggering the current speed formed.

The rotary current is shown in Fig. 6 which shows a series of arrows representing the current direction and speed at each hour. Offshore rotary currents which are originally semidiurnal reiterate the elliptical pattern every 6 hours and 12 minutes. Furthermore, there are clear relationship times of currents and times of tides in the locality (Antony and Unnikrishnan, 2013; Boon, 2004).

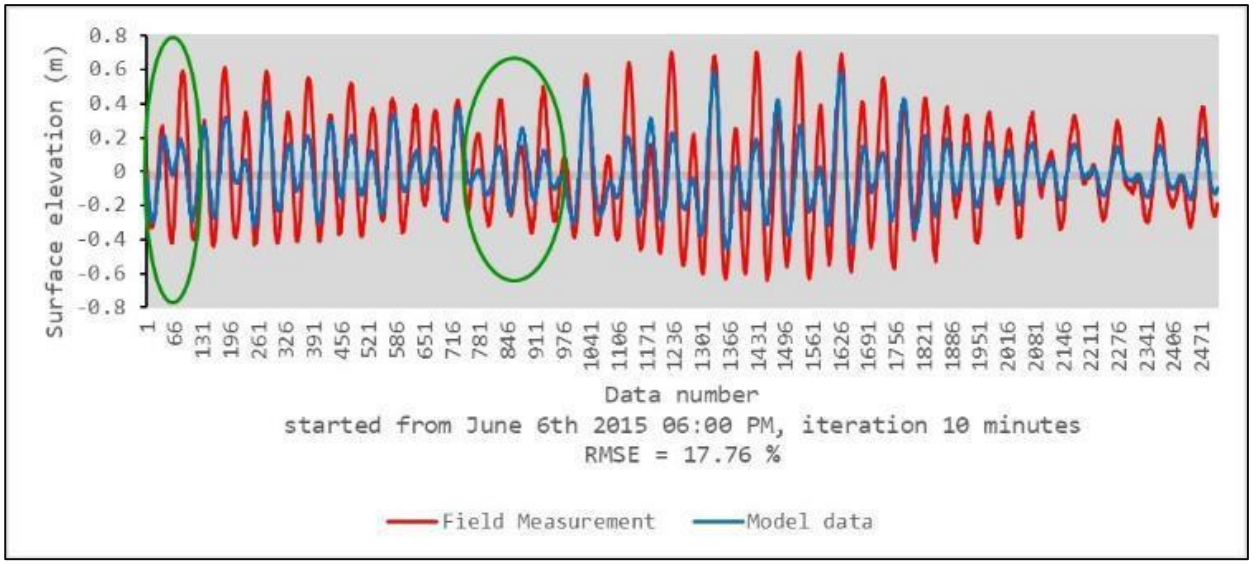

Fig. 6 - Model verification using surface elevation data

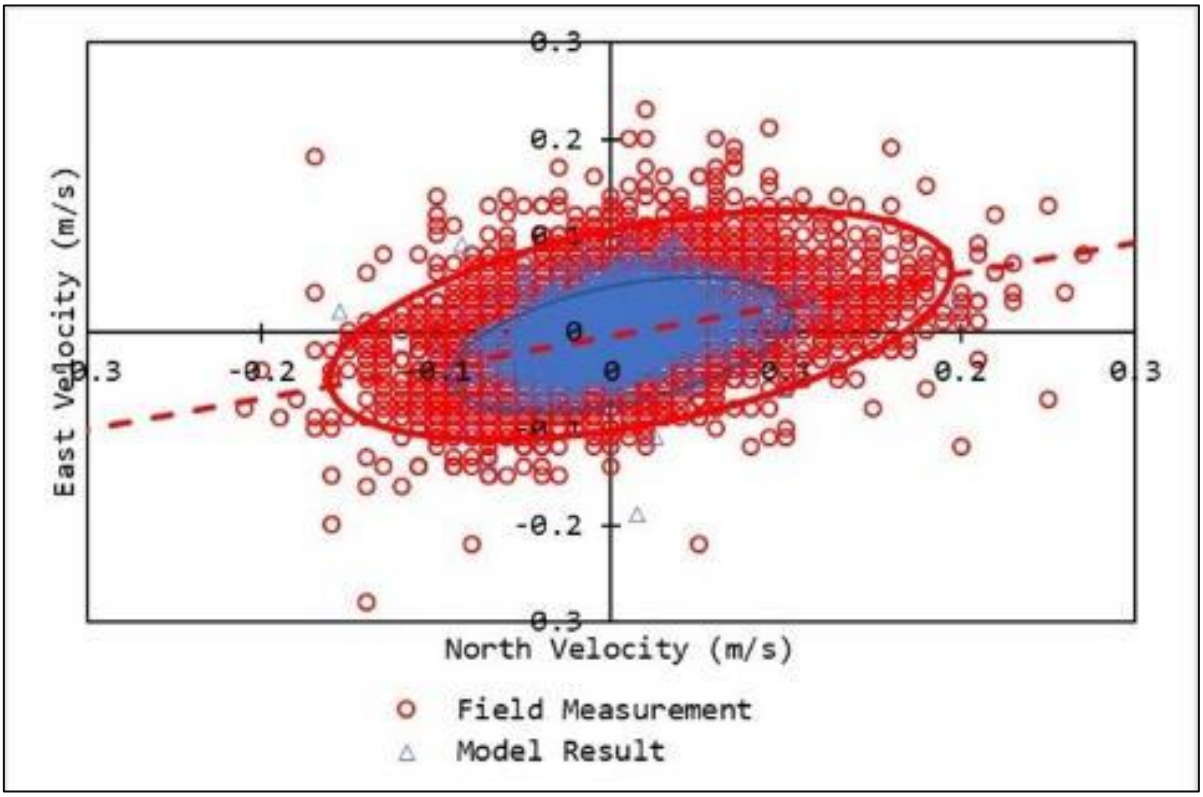

Fig. 7 - Model verification using elliptical velocity component analysis.

3.3 Tidal Current Simulation

During neap tidal conditions (Fig. 8), the current speed ranged from 0-0.023 m.s-1 and 0-0.024 m.s-1 for flood and ebb respectively. At high neap tidal condition, the current flowed from southward and rotated in the bay mouth followed by the increasing speed (ranging from 0.007-0.023 m.s-1) due to narrowed area and the existence of several isles. The direction rotates almost 180 degrees within the bay. Furthermore, the water masses flowed from northward via Cubadak Strait ranged from 0.007-0.012 m.s-1 become weak after passing the narrowed strait, resulting in the low current speed within the bay.

At low neap tidal condition, the current direction predomination flowed toward the southwest. Due to the changes in surface elevation during the replacement of tidal condition, the tidal current flows outer ward the bay through straits around Cubadak Island. The highest speed during ebb tide ranged from 0.004-0.013 m.s-1 right in the bay mouth and Cubadak Strait (Fig. 8). The current speed is slightly different between flood and ebb during neap tidal condition. The current direction within the bay is oppositely rotated almost 180 degrees during the replacement of tidal condition showing that the influence of tidal ellipse parameters takes place. This regime is strongly related to transport mechanism occurred within the bay supported by the bottom morphology creating variations of current speed propagation.

At spring high tidal condition (Fig. 9) the current speed ranged from 0-0.04 m.s-1 which the current direction dominantly towards the northeast. The current flows from sea to inner bay via the straits around Cubadak island. Tidal current from south and west enter the bay significantly suffering deformation of speed and direction. The rendezvous of two sources of water mass occurred within the bay where the mixing of two water masses takes place. The opposite condition happened during low spring tidal condition which the current speed becomes higher ranged from 0-0.05 m.s-1. Tidal current flows separately towards the southwest (out of the bay) due to elevation change. The highest speed is observed in the bay mouth ranged from 0.017 – 0.05 m.s-1.

During the neap tidal condition, the flow velocity is mostly weaker than spring condition because of the moon, sun, and earth gravity forces which are upright resulting in the weakened current generation (Bayhaqi et al., 2018; Lazure et al., 2009; Van Rijn, 2011). The long tidal wave from the deeper ocean will propagate and release the energy in the shallower waters, resulting in the tidal dominated coastal. In the semi-enclosed area of Mandeh Bay, tidal regime takes place which rotates as the elevation changes caused by earth rotation and astronomical forces alteration. The rotation is reiterated according to the tidal type which will move in and out of the bay. This strongly influences turbulence, mixing, and water mass dynamic as well (Bayhaqi et al., 2018).

Tidal current penetrates deeper during ebb than flood tide which causes a significant variation of distributed materials over the ebb-flood tidal cycle, resulting in the insignificant residual changes. This shows that at low tidal condition both neap and spring the transport mechanism is maximally supported by the higher current speed. The strongest currents are observed in the bay mouth where the tidal current patterns are topographically influenced by the shallow subtidal delta platform (the existence of Sutan, Sironjong Gadang, and Sironjong Ketek islands). Consequently, local differences in tidal current pattern and drift velocities contribute to the residual sediment transport within the bay. This is obvious why sedimentation issues are the main problem occurred in Mandeh Bay that directly disrupt the fisheries and marine tourism activities.

Tidal current propagations are strongly influenced by the bathymetry profile. Mandeh Bay categorized into shallow water area which the morphology is uneven ranged from 0-214.54 meters depth. This uneven profile induces the variability of bottom friction which has a big role in hampering the surface current flow. Bottom friction also controls the magnitude of velocity components which it varies over the seabed depended on the bathymetry profile (Efield and Gordon, 2002). When the surface elevation decreased and the current speed enhanced, bottom friction becomes stronger triggering turbulence and mixing in the water column.

3.4 Tidal current ellipse parameters analysis

Fig. 10 depicts the two major semidiurnal and the two major diurnal tidal constituents from our harmonic analysis of tidal current simulation. The reference ellipse for two major semidiurnal tidal constituents has 0.1 m.s-1 radius, while for two major diurnal tidal constituents the radius only 0.05 m.s-1. The predominant constituent is M_2 which is the principal Lunar semi-diurnal tidal constituent.

Overall, M_2 semi-minor axes are primarily negative which most ellipses rotate clockwise. The counterclockwise rotated M_2ellipses are very narrow with semi-minor axes not exceeding 0.01 m.s-1. The maximum phase of tidal current M_2 ranges from 109-117 degrees within the bay and 118-181 degrees in the bay mouth. There is a general increase of the phase values eastward, with several exceptions at some of the southernmost ellipses within the bay and in the bay mouth, where the pattern is fickler. This condition probably is influenced by the bottom morphology and the other physical factors taking place locally such as internal tides that possibly occurred due to the existence of several basins and trenches in the surrounding (Mller et al., 2012).

The second most obtrusive constituent is S_2 which is the principal Solar semi-diurnal tide. The maximum S_2current speed approximately one third the speed of M_2. The highest speeds of S_2 have also observed in the bay mouth reached 0.24 m.s-1. The semi-major axes of the S_2ellipses within the bay (excluding the northernmost ellipses) are oriented more/less zonally. The southernmost ellipses beside Mandeh Peninsula are oriented more meridionally. In the bay mouth, the ellipses are oriented along the channel.

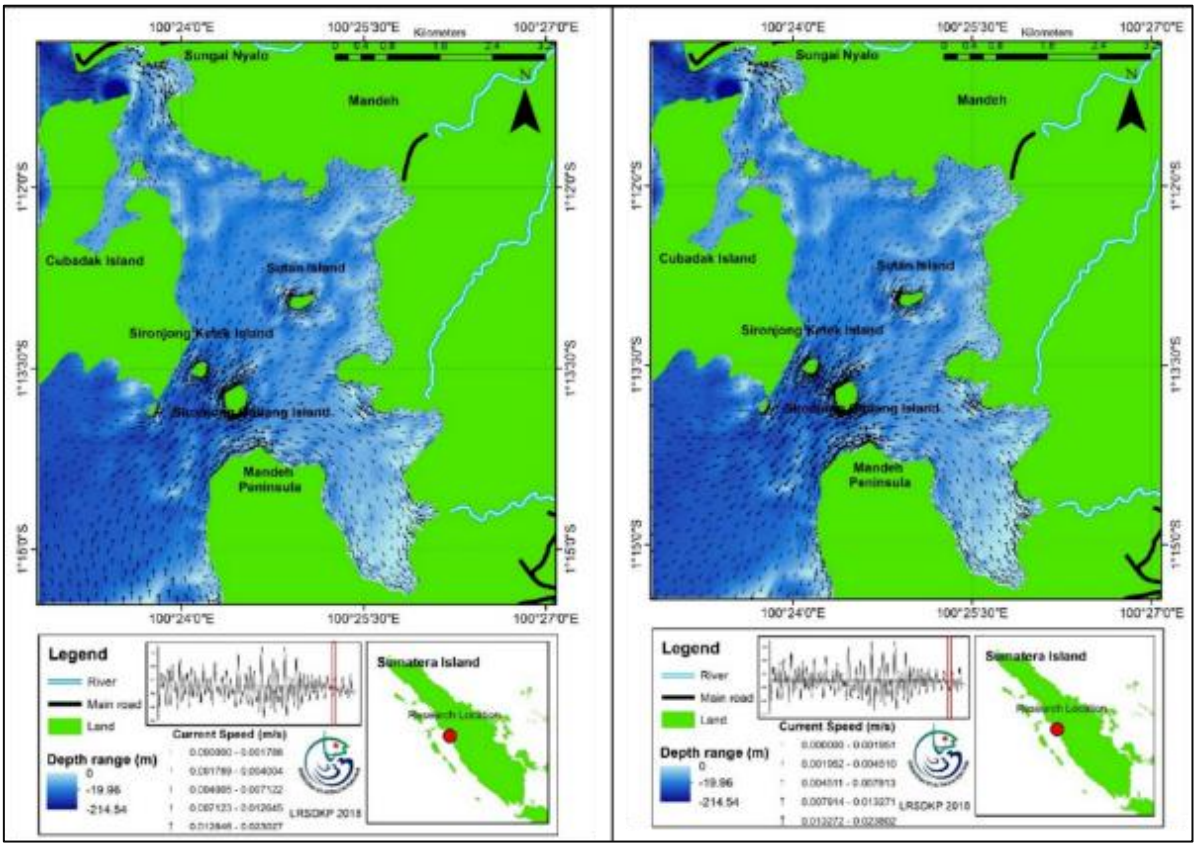

Fig. 8. Tidal current pattern during neap high tidal condition (left) and neap low tidal condition (right)

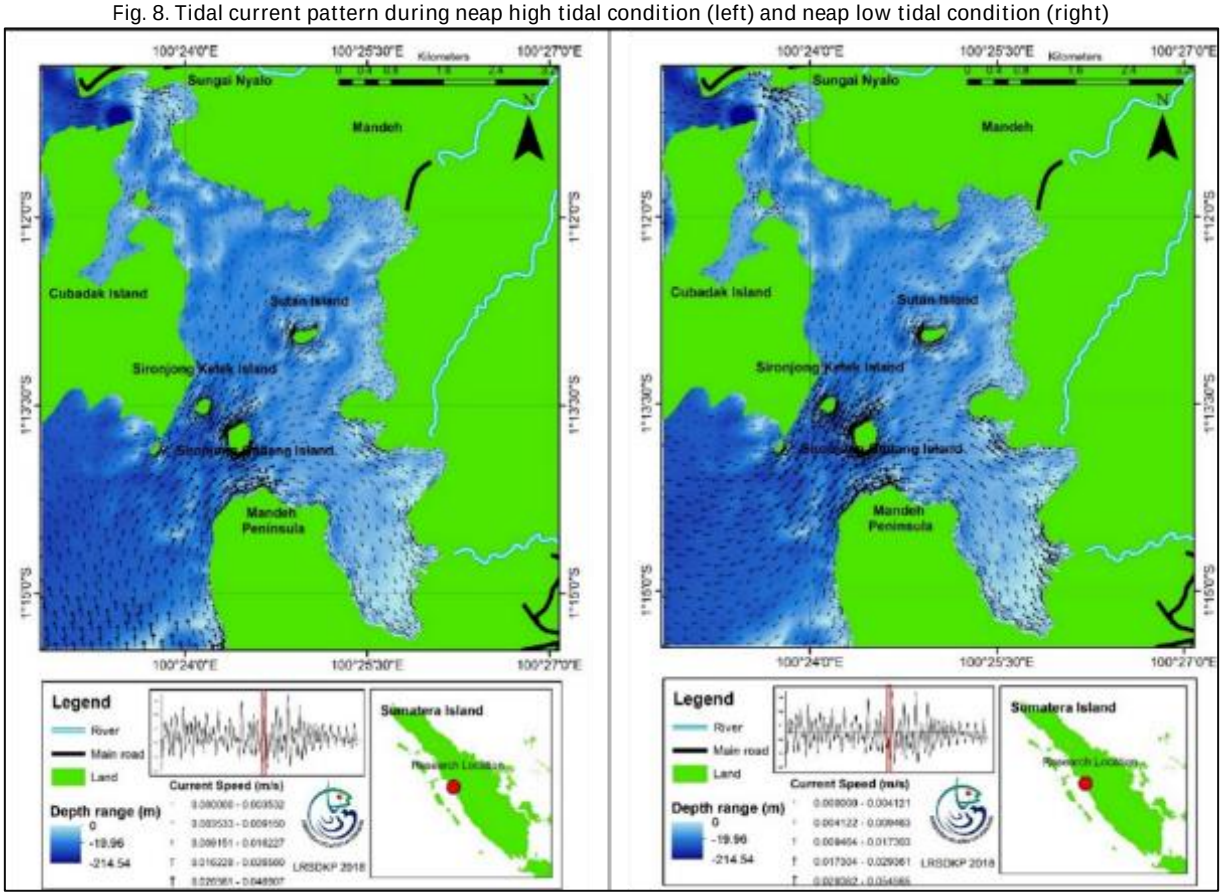

Fig. 9. Tidal current pattern during spring high tidal condition (left) and spring low tidal condition (right).

The phase of S_2 tidal current is quite variable, showing the unclear propagation pattern compared to that we see in the phase of M_2 tidal current, this is also defined by Stanton et al. (2001). However, values in the bay mouth and within the bay ranged from 105 to 283 degrees.

The two main diurnal tidal constituents K_1 and O_1 have the maximum speeds approximately one fifth of M_2 magnitude. Due to the low magnitudes of diurnal tidal constituents, the phase and orientation cannot be well interpreted the tidal current ellipse fluctuations where the accuracy of the derived tidal ellipse parameters decreased as the constituents become weaker (Stanton et al., 2001). The orientation of the ellipses of the diurnal constituents is quite erratic within the bay. In the Cubadak Strait and within the bay beside Mandeh Peninsula, the diurnal ellipses are oriented more meridionally. However, we did not observe the maximum current speeds which tend to be uniform.

The maximal tidal current speeds of N_2 and L_2, the larger lunar elliptic and smaller lunar elliptic constituents, are approximately one fourth and one sixth of the maximal average speed of M_2. The higher harmonic tidal constituents are all relatively weak which the maximal current speed for M_4, M_6, and M_8 are respectively one ninth, one twelfth, and one fifteenth of M_2 magnitude.

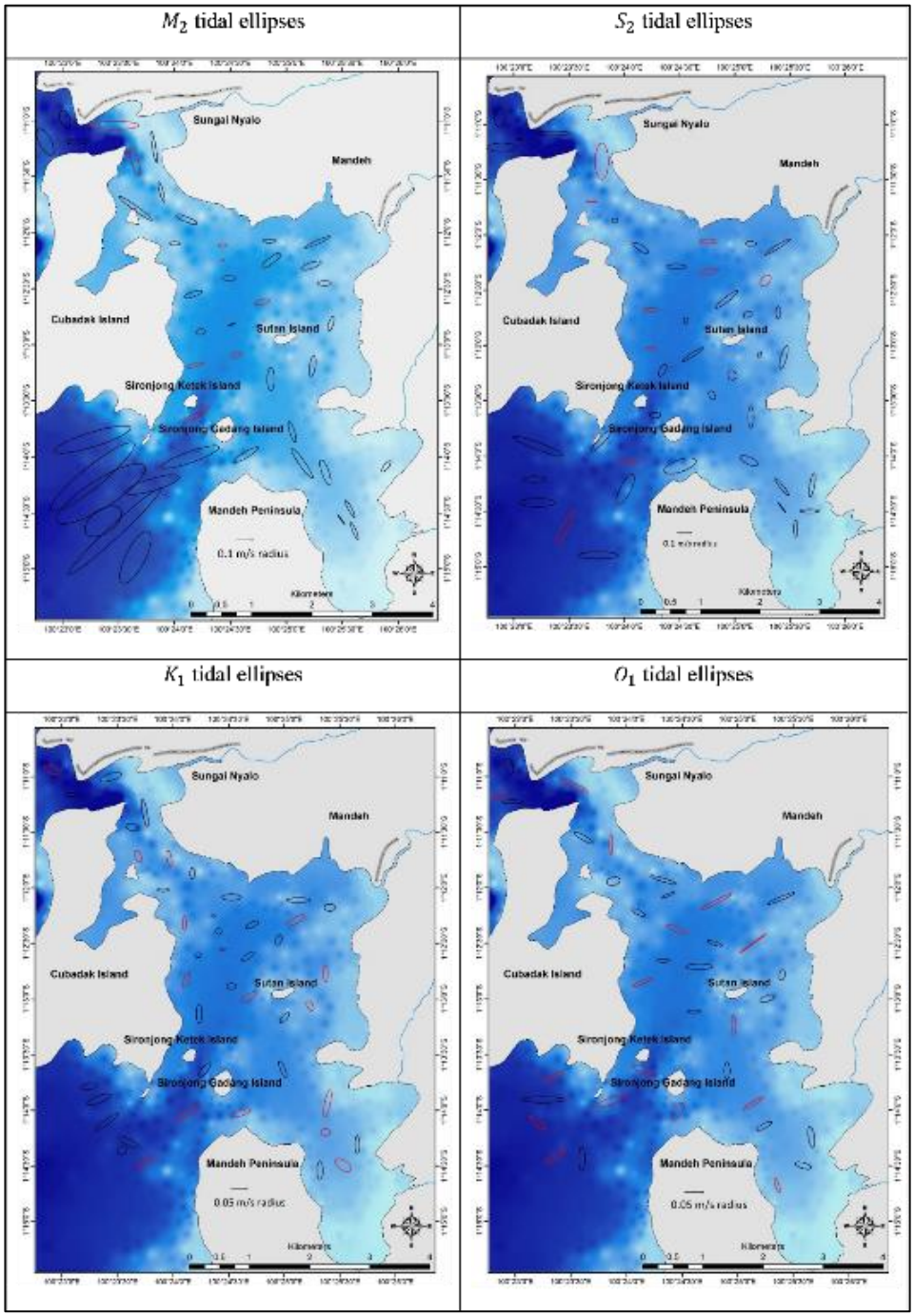

Fig. 10. Tidal ellipses of the two main semi-diurnal tidal constituents (M_2 and S_2) and the two main diurnal constituents (K_1 and O_1). Black ellipses rotate clockwise, and red ellipses rotate counter clockwise.

4. Conclusion

The current speed observed is higher in the surface which gradually rotates clockwise bottom-ward due to the influence of spiral Ekman. The vertical profile of current is reflecting the vertical transport mechanism in Mandeh Bay where the north, east, and up velocity have a special influence of vertical water mass movement. Offshore rotary tidal currents which are originally semidiurnal reiterate the elliptical pattern every 6 hours and 12 minutes which it penetrates deeper during ebb than flood tide causing a significant variation of distributed materials over the ebb-flood tidal cycle, resulting in the insignificant residual changes.

The strongest current speeds are observed in the bay mouth where the tidal current patterns are topographically influenced by the shallow subtidal delta platform (the existence of Sutan, Sironjong Gadang, and Sironjong Ketek Islands). This condition also affects the elliptical variation of tidal current constituents where Mandeh Bay is predominated by semidiurnal constituents (M_2 and S_2). The current speed of M_2 is the highest at all which the S_2 speed is averagely one third of M_2 magnitude. Thus, this may trigger a higher sediment distribution and accumulation within the bay because of the twice tidal oscillations entering the bay.

This study will be more appropriate if the ADCP measurement is fully covering the bay by which the vessel moored ADCP survey is possible to be conducted. The estimated tidal constituents which have relatively high uncertainties, lead us to conclude that the tidal cycle is well replicated in our analysis, but we will lack precision due to the lesser constituents. This study only used the model result that is an approach, so that integrated field measurement of current is essential for further studies either in Mandeh Bay or the other possible locations.

Acknowledgment

We acknowledge and are grateful to the Research Institute for Coastal Resources and Vulnerability's (RICRV's) 2018 research funding for West Sumatera, the local government of Pesisir Selatan, and the Head of RICRV Nia Naelul Hasanah Ridwan, undergraduate marine science student of Riau University Okse Tudela Indra who helped in the filed data acquisition and processing, and those who supported the completion of this paper, as well as for every institution that supported the completion of the main data.

References

Antony, C., Unnikrishnan, A.S., 2013. Observed characteristics of tide-surge interaction along the east coast of india and the head of bay of bengal. Estuar. Coast. Shelf Sci. https://doi.org/10.1016/j.ecss.2013.08.004

Bábek, O., Grygar, T.M., Faměra, M., Hron, K., Nováková, T., Sedláček, J., 2015. Geochemical background in polluted river sediments: How to separate the effects of sediment provenance and grain size with statistical rigour? Catena. https://doi.org/10.1016/j.catena.2015.07.003

Bayhaqi, A., Wisha, U.J., Surinati, D., 2018. Modeling Tidal Current on Banten Bay During Transitional Monsoons. J. Segara. https://doi.org/10.15578/segara.v14i2.6452

Boon, J.D., 2004. Secrets of the Tide: Tide and Tidal Current Analysis and Predictions, Storm Surges and Sea Level Trends, Secrets of the Tide: Tide and Tidal Current Analysis and Predictions, Storm Surges and Sea Level Trends. https://doi.org/10.1016/C2013-0-18114-7

Chen, J.L., Hsu, T.J., Shi, F., Raubenheimer, B., Elgar, S., 2015. Hydrodynamic and sediment transport modeling of New River Inlet (NC) under the interaction of tides and waves. J. Geophys. Res. Ocean. https://doi.org/10.1002/2014JC010425

Chen, W., de Swart, H.E., 2018. Longitudinal variation in lateral trapping of fine sediment in tidal estuaries: observations and a 3D exploratory model. Ocean Dyn. https://doi.org/10.1007/s10236-018-1134-z

Duhec, A. V., Jeanne, R.F., Maximenko, N., Hafner, J., 2015. Composition and potential origin of marine debris stranded in the Western Indian Ocean on remote Alphonse Island, Seychelles. Mar. Pollut. Bull. https://doi.org/10.1016/j.marpolbul.2015.05.042

Ffield, A., Gordon, A.L., 2002. Tidal Mixing Signatures in the Indonesian Seas. J. Phys. Oceanogr. https://doi.org/10.1175/1520-0485(1996)026<1924:tmsiti>2.0.co;2

Foreman, M.G.G.G.G., 1978. Manual for tidal currents analysis and prediction. Pacific Mar. Sci. Rep. 78-6.

Hanebuth, T.J.J., Zhang, W., Hofmann, A.L., Löwemark, L.A., Schwenk, T., 2015. Oceanic density fronts steering bottom-current induced sedimentation deduced from a 50ka contourite-drift record and numerical modeling (off NW Spain). Quat. Sci. Rev. https://doi.org/10.1016/j.quascirev.2015.01.027

Hermon, D., 2016. The Strategic Model of Tsunami Based in Coastal Ecotourism Development at The Strategic Model of Tsunami Based in Coastal Ecotourism Development at Mandeh Regions , West Sumatera , Indonesia. J. Environ. Earth Sci. 6, 40–45. https://doi.org/https://doi.org/10.7176/JEES.2016.001

Hidayat, R., Rozamuri, M.F., 2016. Comparison of Grain-Size Profile and Depositional Process in Mandeh and 1, 36–42. https://doi.org/10.22146/jag.26958

Lazure, P., Garnier, V., Dumas, F., Herry, C., Chifflet, M., 2009. Development of a hydrodynamic model of the Bay of Biscay. Validation of hydrology. Cont. Shelf Res. https://doi.org/10.1016/j.csr.2008.12.017

MIler, M., Cherniawsky, J.Y., Foreman, M.G.G., Von Storch, J.S., 2012. Global M<inf>2</inf> internal tide and its seasonal variability from high resolution ocean circulation and tide modeling. Geophys. Res. Lett. https://doi.org/10.1029/2012GL053320

Mukhtar, P.D., Rudiyanti, S., Purwanti, F., 2016. Analysis of Tourism Suitability in Nyalo Coast (Mandeh Region) Pesisir Selatan Regency, West Sumatera. Manag. Aquat. Resour. J. 5, 420–426.

Poulain, P.M., 2013. Tidal currents in the Adriatic as measured by surface drifters. J. Geophys. Res. Ocean. https://doi.org/10.1002/jgrc.20147

Qarnain, A.G.D., Satriadi, A., Setiyono, H., 2014. Analysis of Spring and Neap Tides Influence on the sedimentary rate in Timbulsloko Waters, Demak. J. Oceanogr. 3, 540–548.

Rath, S., Vinayachandran, P.N., Behara, A., Neema, C.P., 2017. Dynamics of Summer Monsoon Currents around Sri Lanka.

Stanton, B.R., Goring, D.G., Bell, R.G., 2001. Observed and modelled tidal currents in the New Zealand region. New Zeal. J. Mar. Freshw. Res. https://doi.org/10.1080/00288330.2001.9517010

Van Rijn, L.C., 2011. Analytical and numerical analysis of tides and salinities in estuaries; Part I: Tidal wave propagation in convergent estuaries, in: Ocean Dynamics. https://doi.org/10.1007/s10236-011-0453-0

Vindenes, H., Orvik, K.A., Søiland, H., Wehde, H., 2018. Analysis of tidal currents in the North Sea from shipboard acoustic Doppler current profiler data. Cont. Shelf Res. 162, 1–12. https://doi.org/10.1016/j.csr.2018.04.001

Wang, A. jun, Ye, X., Xu, X. hui, Yin, X. jie, Xu, Y. hang, 2018. Settling flux and origin of particulate organic carbon in a macro-tidal semi-enclosed embayment: Luoyuan Bay, Southeast China coast. Estuar. Coast. Shelf Sci. https://doi.org/10.1016/j.ecss.2017.03.023

Yanagi, T., Shimizu, M., Nomura, M., Furukawa, K., 2003. Spring-neap tidal variations of residual flow in Tokyo Bay, Japan. Cont. Shelf Res. https://doi.org/10.1016/S0278-4343(03)00102-X